A parametric study on the fatigue life of turnout crossings using the finite element approach

Xin, L; Markine, VL

DOI
10.4203/ccp.110.119

Publication date
2016

Document Version
Accepted author manuscript

Published in
Proceedings of the 3rd international conference on railway technology: Research, development and maintenance

Parametric Study on Fatigue Life of Turnout Crossing Using Finite Element Approach

Xin, Lizuo; Markine, Valeri

Publication date
2017

Document Version
Accepted author manuscript

Published in
The International Journal of Railway Technology

Citation (APA)
Xin, L., & Markine, VL. (Accepted/In press). Parametric Study on Fatigue Life of Turnout Crossing Using Finite Element Approach. The International Journal of Railway Technology, 6.

This paper has been accepted by The International Journal of Railway Technology
http://www.saxe-coburg.co.uk/ijrt/
Accepted date: Feb 1st , 2017

Parametric Study on Fatigue Life of Turnout Crossing Using Finite Element Approach

L. Xin and V.L. Markine

Delft University of Technology, Delft, The Netherlands

Abstract

Railway turnouts (switches and crossings) are important elements in the railway infrastructure that provide flexibility of the system and guide the railway traffic. However, due to the high impact forces, severe damage to the turnout crossing can frequently be observed. In this paper parametric studies are performed to investigate the effects of different railpads, friction coefficients and traveling directions on the dynamic behaviour of the turnout crossing. First, the dynamic behaviour is analysed using the explicit finite element method accounting for non-linear material properties (plasticity) of rails. From the numerical simulations the dynamic responses such as contact forces, stress and strain distributions in rails, sleepers and ballast are obtained. After that on the basis of the obtained responses rail fatigue analysis is performed. A critical plane and energy density based fatigue analysis approach is used to assess the crossing performance under various conditions of the parametric studies. The performance is estimated by the predicted fatigue life to crack initiation in the crossing rail. The results of these parametric studies are presented and discussed.

Keywords: Turnout crossing, dynamics, wheel-rail contact, explicit finite element modeling, fatigue analysis

1. Introduction

1.1. Turnout crossing

Railway turnouts are one of the most important elements in the track system, since different tracks intersect at turnouts and the railway traffic is guided by turnouts. A typical turnout consists of a switch panel, a closure panel and a crossing panel. In contrast to a normal track wherein the rail profile remains constant, the rail cross-section in the crossing section of a turnout is changing. During the wheel passing over the turnout crossing, the wheel load is to be transferred from the wing rail to the crossing nose, which is named as facing direction and the other direction is named as trailing direction. Due to the geometrical discontinuities of turnouts, such as the gap between wing rail and crossing nose, high impact forces are excited here during the wheel passage. Severe rail damage and fast degradation of the material is thus observed. Therefore, a number of design modifications have been implemented to reduce the impact forces and damage to the crossing nose, such as the usage of the movable frog in high-speed line as well as the enhancement of the material properties in turnouts. However, it remains difficult to significantly reduce the damage to conventional crossings which are still widely used, e.g. in the Netherlands. Consequently, a comprehensive understanding and solutions to crossing related problems are urgently needed.

1.2. Influential parameters

There are several parameters that may influence the wheel/crossing interaction, among which the geometry and material properties of the wheel and crossing play important roles. Several research studies have been conducted on the effect of the crossing geometry, such as the optimization of the crossing geometry, which proves that the slightly changed geometry can lead to either great improvement or degradation in wheel/crossing interaction [1,2]. On the other hand, crossing material is closely related to the amount of wear and rolling contact fatigue (RCF) of the wheel and crossing. Many studies related to crossing material have been conducted. For example, three crossing nose materials were studied by the multi-scale FE approach, in which the crack development and growth using the three materials were obtained and compared in [3]. Experimental investigations of fatigue properties were conducted of casted austenitic manganese steel that was used in railway turnouts and crossings [4]. In [5] a crossing nose model with a type of weld defect that generating a layer of martensite in the material was simulated and analysed.

Except for the above-mentioned factors, there are several parameters that may also affect the wheel and crossing interaction, such as the rail supporting stiffness, friction coefficient and traveling directions. The effect of the vertical elastic track properties on the dynamic behaviour of the turnout crossing was studied in [6,7] using the two-dimensional (2-D) finite element software DARTS_NL. However, modeling of the substructure such as railpads and sleepers was simplified, which was incapable for stress and strain solutions in these components. As for the friction conditions between the wheels and rails, they can vary greatly and can significantly affect the wheel-rail interaction. On one hand, the adhesion in the wheel-rail interface must be sufficient to ensure the ability to brake and accelerate; on the other hand, it should be low to keep the energy consumption down [8]. Furthermore, the

friction coefficient between the wheel and rail should not vary too much so as to avoid stick-slip oscillation, which may induce rail corrugation leading to noise and poor comfort [9]. Research studies have been frequently conducted on it, for instance, the damage on turnout influenced by a stochastic spread in traffic parameters including friction coefficient was analysed in [10], but the responses related to the interface stress and strain were not taken into account over there. As for the traveling direction, it was observed in the Dutch railway network that it can also have a great effect on the crossing behaviour. So that, in a 1:9 (manganese steel) turnout crossings, fast degradation was observed when the train travelled in trailing direction with the speed of 140km/h [11]. Besides the increased damage to the crossings, considerable geometry degradation was observed in these turnouts. Also, opposite to the high impact generated on the crossing nose in the facing move, trailing move results in highly possible damage on the wing rail. Therefore, it is crucial that the dynamic behaviour of both crossing and wing rails is investigated in trailing direction. Numerical analysis of a 1:15 turnout was performed in [12] that contact forces in the trailing direction of a train with three velocities were simulated and compared, which showed that higher impact was generated on the wing rail as the velocities increased. However, the lateral movement of the wheel was prescribed in the model that may strongly affect the wheel transition behaviour. All these shortages lead to the necessity to simulate the effects of the influential parameters on crossings and propose the criteria to assess the crossing performance.

1.3. Fatigue life analysis

Rolling contact fatigue (RCF) has been a severe problem in turnout crossings due to the high impact forces acting on the rails. In the Netherlands, RCF in turnout crossings causes most of the operation disturbance of the turnout. During the last 6 years the RCF damage on track was significantly decreased (more than 50%), however this reduction was not noticeable at the turnouts. The replacement budget reaches 6.4 million per year, thus solutions for the RCF related problems in turnout crossings are urgently needed. Therefore, to evaluate the fatigue life of the turnout crossings, a fatigue analysis approach predicting the crack initiation plane and the fatigue life to crack initiation has been developed in [13]. In the previous research the approach has been used to evaluate the crack initiation plane and number of cycles to fatigue crack initiation of the crossing at different depth and longitudinal positions, which showed good correspondence to the field observations.

1.4. Analysis procedure

In this paper, the effects of the

- railpads stiffness
- friction coefficients
- traveling directions

on turnout crossing behaviour are analysed. All the other factors such as crossing geometry and material, wheel load as well as vehicle velocities remain stable, so that in Section 4 only one factor is changed at one time. A three dimensional (3-D) explicit FE model (Section 2) developed in [14] is used to obtain the dynamic response of the wheel and crossing interaction, including contact forces, stress and strain distributions of the rails and substructure (Section 4). The responses are used as input into the fatigue model (Section 3) to determine the crack initiation planes as well as the fatigue life of the crossing nose (Section 5). This approach is applied in the parametric studies and the comparisons of these parameters are conducted to assess the crossing performance under different conditions.

2. Finite element model

In this paper, a 3-D explicit FE model (Figure 1a) with the implementation of elastic-plastic nonlinear isotropic and kinematic hardening material model developed in [14] is used to simulate the dynamic response of a whole wheelset while it is passing a crossing. The turnout modelled here is the curved one with the radius of 725m and the crossing angle of 1:15. The crossing nose in the model is built using four main cross-sections as they are defined in the drawings from the manufacturer (Figure 1b). To remain the ability to capture the wheel and crossing interaction and meanwhile reduce the calculation time, the model consisting of a crossing section of 4540mm long, in the main direction of a left-handed turnout is considered. The wheelset with S1002 unworn wheel profile is placed at a position of 376mm on the wing rail before the crossing nose, which will roll over the crossing during the simulation without any lateral constraint. To provide the support to the wheelset, stock rail with 54E1 rail profile is also included in the model.

The rails including wing rail, crossing and stock rail are supported by the 10 mm thick railpads, concrete sleepers with the spacing of 600 mm and ballast bed with the thickness of 350 mm. All the components are modelled using solid elements, which are capable for the stresses and strain distributions in the track components such as sleepers and ballast. Fine mesh of $1.5\text{mm} \times 1.5\text{mm}$ is used for the wheel-rail contact region, i.e. the wheel tread, top of the crossing nose, wing rail and stock rail (Figure 1c). The material properties of the crossing are modelled by an elasto-plastic isotropic and kinematic hardening material model, which is based on the Lemaitre and Chaboche (1990) material model. It is well suited to model the nonlinear isotropic and kinematic plasticity and it accounts for cyclic hardening and ratcheting. Other components are modelled as linear elastic. The transmitting boundary is applied to both end of the ballast layer to model the semi-infinite domain.

During the simulation, the wheelset moves along the crossing with the translational velocity of 130 km/h and the angular velocity of 78.5 rad/s. The axle load of 150kN has been applied. The implicit stress initialization stage is applied before the explicit analysis to achieve the stabilization of the system. The simulation time of 50 ms has been chosen which is sufficient for analysis of the wheel/rail impact. The railpad stiffness of 854 MN/m, friction coefficient of 0.2 and the facing

direction have been modelled in the reference simulations. Details of the model is introduced and discussed in [14].

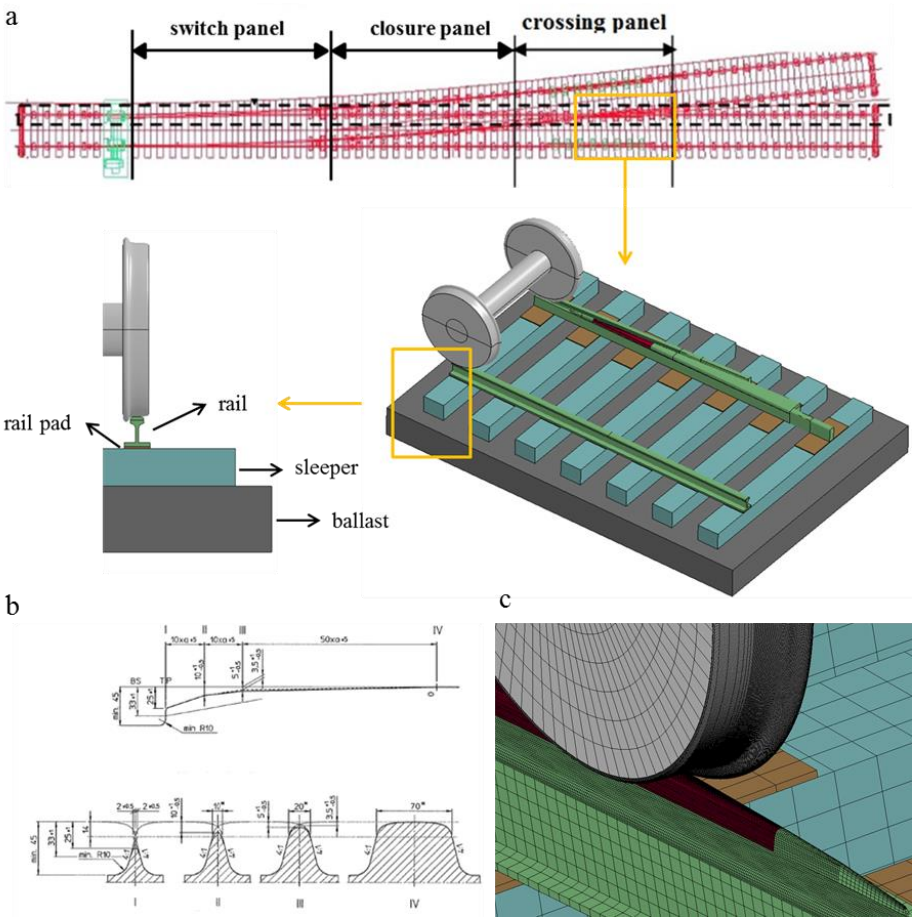

Figure 1. (a) schematic representation of the finite element model, (b) drawing from the manufacturer, (c) mesh of the wheel, crossing and wing rail

3. Fatigue model

Using the stress and strain state obtained from FE modeling, fatigue life prediction of the crossing can be performed. The fatigue life of the rails is defined as the time to RCF crack initiation. In predicting the crack initiation plane, a combined energy density and critical plane based approach for low cycle fatigue problems (proposed by Jiang and Sehitoglu (J-S)[15]) is used to predict the fatigue life of the crossing. In this criterion, it considers that both normal and shear components of stress and strain on the critical plane contribute to the damage of the material. The damage/fatigue parameter FP is defined as:

$$FP = \langle \sigma_{max} \rangle \frac{\Delta \varepsilon}{2} + J \Delta \gamma \Delta \tau \quad (1)$$

where ⟨ ⟩ is the MacCauley bracket, $\langle x \rangle = 0.5(|x| + x)$; σ_{max} is the maximum normal stress; $\Delta\varepsilon$ is the normal strain range; $\Delta\gamma$ is the shear strain range; $\Delta\tau$ is the shear strain range; J is the material-dependent constant. Through a tensor rotation for the stress and strain, the maximum FP and the critical plane are determined by surveying all the possible planes at a material point. The energy density is computed as FP on every material plane and for every increment of loading. The critical plane is defined as the plane with the maximum FP. Considering the possible tensile and shear cracking mode, the fatigue life to crack initiation, N_f, is computed on a critical crack plane:

$$FP_{max} =$$

$$\begin{cases} \left(\langle\sigma^{max}\rangle\frac{\Delta\varepsilon}{2} + J\Delta\tau\Delta\gamma\right)_{max} = \frac{(\sigma_f')^2}{E}(2N_f)^{2b} + \sigma_f'\varepsilon_f'(2N_f)^{b+c} & (2a) \\ \left(\langle\sigma^{max}\rangle\frac{\Delta\varepsilon}{2} + J\Delta\tau\Delta\gamma\right)_{max} = \frac{\left(\tau_f'\right)^2}{E}\left(2N_f\right)^{2b} + \tau_f'\gamma_f'\left(2N_f\right)^{b+c} & (2b) \end{cases}$$

where E, G are the elastic/shear modulus; σ_f', τ_f' are the tensile/shear fatigue strength coefficients; ε_f', γ_f' are the tensile/shear fatigue ductility coefficients. By analysing the stress and strain components in FP, the proper form of the model can be selected from Eq.(2a) and Eq. (2b)

The effects of different railpads stiffness, friction coefficients as well as the traveling directions are analysed by this approach. In each case, using the results from FE simulations the critical positions on the crossing nose susceptible to crack initiation are determined first. Then, using the fatigue model the number of cycles to fatigue crack initiation is calculated for each case, based on which the corresponding crossing life is determined and the effects of these parameters are evaluated.

4. Dynamic response

The dynamic responses such as contact forces between the wheel and rail in three directions, displacements and stress/strain distributions in wheel, rails and substructures can be obtained from the FE modeling. Therefore, in the parametric studies the simulations were performed first and the performance of the turnouts was assessed using the following response quantities:

- Contact forces between wheel and wing rail/crossing/stock rail
- Von Mises (VM) stress and effective plastic strain in the rails, sleepers and ballast
- Transition behaviour, i.e. the start and end position of the transition, wheelset movement
- Surface shear stress and pressure, friction energy dissipation

These results are presented in this Section. Based on these results the fatigue life to crack initiation for each study is analysed in Section 5.

4.1.Elasticity of railpads

A number of studies [1,7,16] have proved that tuning the elastic track properties such as railpads and under sleeper pads can significantly reduce the dynamic forces acting on the rails. However, for the wheel-crossing impact, these effects have not been investigated at the stress and strain level yet, which is closely related to the fatigue life of the crossing. In this study, in order to determine the level of the elasticity that should be applied to reduce the dynamic forces acting on the crossing nose, two values of the railpads stiffness are investigated. One is the normal stiffness and the other is very soft pad as it was investigated in [2]. The positions of the varied railpads and their properties are shown in Figure 2 and Table 1. In the case of v02, the stiffness of all railpads in the model under the crossing nose has been varied ($R_1 \sim R_7$). The contact forces between the wheel and crossing as well as the stress results in sleepers and ballast of case v01 and v02 are compared.

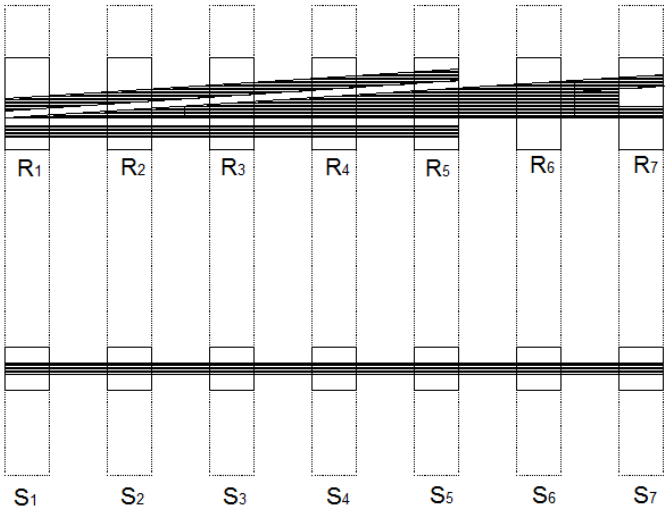

Figure 2. Numbering of the railpads and sleepers in the model

Var.	Pads name	Varied pads num.	Stiffness (MN/m)	Corresponding elastic modulus (Pa)
v01	Normal pad	-	854	2.4e+8
v02	Soft pad	$R_1 \sim R_7$	40	1.13e+7
v03	Soft pad (local)	$R_1 \sim R_3$	40	1.13e+7/2.4e+8

Table 1. Variation of the railpads stiffness

Since it is the 1:15 crossing that has been investigated, the crossing nose from 0m to 1.05m and the wing rail starting from -0.3m in front of the nose point are shown in the following figures. The wheel-rail vertical contact forces are plotted in Figure

3a. It shows that the impact force on the crossing nose (right peak in the figure) is reduced using the soft pads and is more distributed over the crossing. Also, the impact position is shifted further along the crossing. Furthermore, in this study the Von Mises (VM) stress is chosen as the one of criteria to assess the crossing performance. The position with the maximum VM stress is determined as the critical position P_{cr} along the rail. The maximum VM stresses in the crossing distributed along the longitudinal direction of the rail are shown in Figure 3b, with the transition area shown in the dotted line. Transition is the area that the wheel load is transferred from the wing rail to the crossing nose in the facing direction. It should be noted that since the transitions vary little in both cases (intersecting area of wing rail and crossing contact forces in Figure 3a), only the transition of normal pad is shown in Figure 3b. It can be seen that similar to the contact forces distribution, the maximum VM stress is more distributed on the crossing and is slightly reduced at the crossing front (0.3m-0.7m). At the crossing rear (0.7m-1.05m) the value increases, due to the fact that the impact location is shifted backwards when using soft pads, which is corresponding to the contact force distribution.

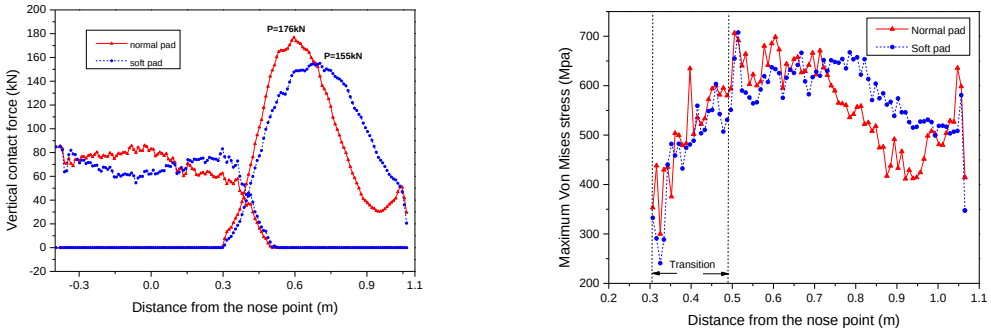

a b

Figure 3. Results of railpads stiffness variation: (a) vertical contact force of stock rail, wing rail and crossing nose, (b) maximum VM stress distribution on the crossing

Besides the contact conditions at the wheel-rail interface, the stresses in sleepers and ballast are also taken into account to investigate the effect on the impact to the substructure. Figure 4 plots the maximum VM stresses in the four sleepers and ballast, where the numbering and positions of the sleepers are shown in Figure 2. Figure 4a shows that using soft pads, the maximum VM stresses in all sleepers occur later. The VM stresses in s_1, s_2 and s_3 are significantly reduced when using soft pads, while for s_4 the stresses become higher due to the later impact. The maximum VM stress in ballast is also reduced by the soft pad. The reduction as well as the increment in four sleepers and ballast is listed in Table 2.

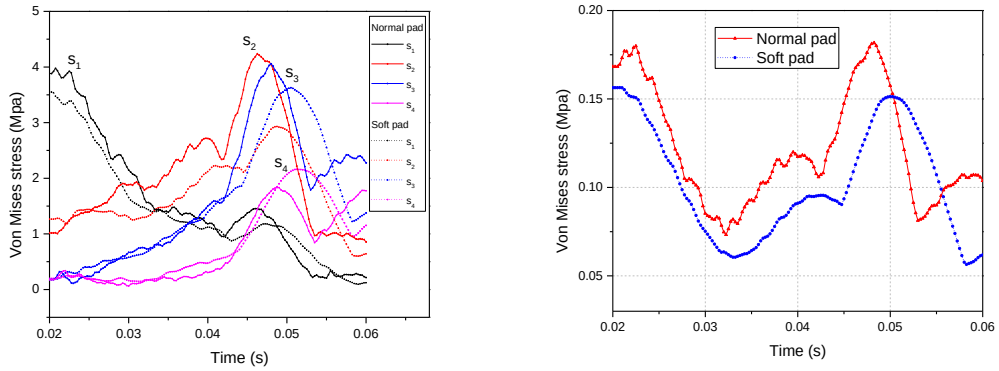

a b

Figure 4. Results of railpads stiffness variation: maximum VM stress in (a) four sleepers, $s_1 \sim s_4$, (b) ballast

The maxima of the results for the two railpads are compared in Table 2. It can be seen that the position where the maximum vertical contact force occurs is later on the crossing by 108mm. The vertical contact force, maximum sleeper (s_1 to s_3) and ballast stresses are reduced, where the reduction of s_2 is the most significant. In both cases the wheel positions at the moment when the maximum VM stress in s_2 occurs are near the position of impact, which means that by reducing the stiffness of the railpad, the stress in the most critical sleeper (s_2) can be significantly reduced (30%).

	Max vertical contact force (kN)	Max pressure (Mpa)	Position of max vertical force (mm)	Max sleeper stress (Mpa)				Max ballast stress (Mpa)
				S1	S2	S3	S4	
Normal pad (v01)	176.8	1227	596	3.98	4.23	4.06	1.83	0.18
Soft pad (v02)	155.0	1169	704	3.55	2.93	3.63	2.16	0.15
Reduction by soft pad	12.3%	4.7%	-108mm (backward)	10.8%	30.7%	10.6 %	-18.0 %	16.7%

Table 2. Results of railpads stiffness variation

According to the previous study [7] of the optimization of elastic track properties of turnout crossings, it was concluded that the optimum track elasticity of the turnout depends on the locations of the elastic elements along the crossing. In the transition area, i.e. from the sleeper before the crossing nose to two sleepers afterwards, softer pads should be implemented. At the crossing front (before R_1 in Figure 2) as well as the rear (R_4 to R_7), the stiffness should remain a higher value. Therefore, in this model only the railpads from R_1 to R_3 are varied using the

stiffness of soft pad (v03), while the other railpads remain the stiffness of the normal pad. The properties are listed in Table 1 as v03.

The vertical contact force and maximum VM stress are shown in Figure 5. From the contact forces between the wheel and wing rail (before 0.4m in Figure 5a), it can be seen that in v03 more vibration is introduced in the wheel-crossing contact which results in the increment of the maximum vertical contact force (around 0.6m), also the wheel and crossing contact in v03 occurs a bit later. Similar results are found in Figure 5b that at the crossing front (0.3m-0.4m) the VM stress is reduced. The stresses at the impact positions are comparable, while the stresses after the impact are reduced in v03. Therefore, it can be concluded that compared with v02, the stress state in the wheel-crossing contact has been greatly changed by varying the railpads stiffness locally. Reducing the railpads stiffness under the crossing nose ($R_1 \sim R_3$) may delay the wheel and crossing contact so that the crossing front is subjected to less impact. Therefore, applying the soft railpads only under the crossing nose can be beneficial to reduce the impact on the crossing.

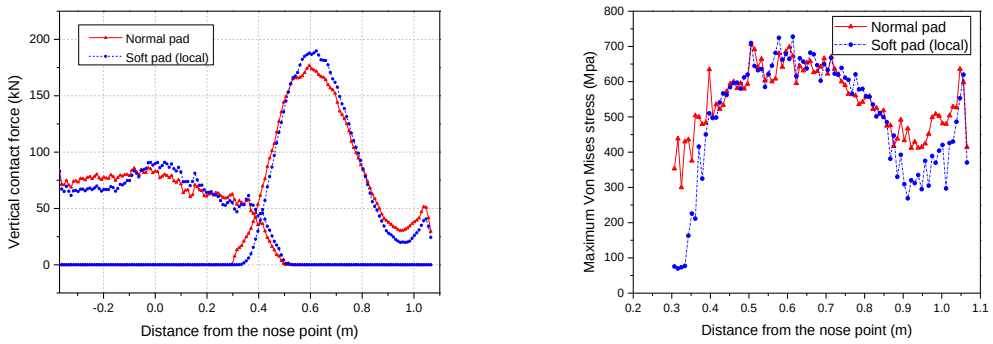

a b

Figure 5. Results of railpads stiffness variation (v01 and v03): (a) vertical contact force of wing rail and crossing nose, (b) maximum VM stress distribution on the crossing

4.2. Friction coefficient

For the steel-steel contact under dry, clean conditions, the friction coefficient is approximately 0.6. However, the wheel-rail interface is an open system, so that contaminants can enter the interface and affect the friction levels, making the wheel-rail adhesion too high or too low [8]. Table 3 shows the friction coefficient measured under different conditions. Therefore, in this section, two cases of friction coefficients of 0.2 and 0.7 representing the raining and dry conditions are studied. All the other parameters are kept as the same in the preceding section.

Conditions	Temperature (°C)	Friction coefficient
Sunshine, dry rail	19	0.6-0.7
Recent rail on rail	5	0.2-0.3

A lot of grease on rail	8	0.05-0.1
Damp leaf film on rail	8	0.05-0.1

Table 3. Fiction coefficients measured on metro lines using a band-pushed tribometer [17]

Figure 6a shows the maximum VM stress distribution in the crossing, with the two dotted lines representing the transition area. Since it is found that the friction coefficient has little effect on the transition area, only the transition of the reference case is shown. The critical positions on the crossing are determined, which are at P=507mm, 707Mpa ($\mu = 0.2$) and P=533mm, 778Mpa ($\mu = 0.7$), showing that the position of impact is slightly shifted backward by the high friction. Figure 6b shows the effective plastic strain in the crossing after one wheel passage. It can be seen that with higher friction coefficient, the plastic deformation increases a little and is more distributed along the crossing. The position of maximum plastic deformation is shifted backwards for 12mm with $\mu = 0.7$, which is corresponding to the maximum VM stress position. More importantly, it can be seen from Figure 6a that the VM stress value increases at the crossing front (0.3m to 0.55m), just at the transition area. It can be explained by the fact that in the transition area, it is the wing rail that defines the rolling of the wheel. Therefore, the wheel is more likely to roll on the wing rail and slide on the crossing nose, which generates an increasing amount of shear stress and greatly varies the stress state in the crossing. After the wheel rolls over the crossing, the difference of VM stresses in the crossing becomes small, which is due to the fact that the wheel has started rolling only on the crossing. Since in this model no traction is applied to the wheelset, the VM stress is not greatly affected by the friction coefficient.

To verify the conclusion drawn above, the surface shear stresses of both cases at three positions that are $P_1 = 72.2$mm (before the transition), $P_2 = 325.0$mm (in the transition) and $P_3 = 577.7$mm (after the transition) are shown in Figure 7. It can be seen that at P_1, in both cases the surface shear stresses in the wing rail are comparable. At P_2, the surface shear stress in the crossing nose with high friction significantly increases by 159%, while in the wing rail the stress is slightly reduced. At P_3, the difference of the stresses drops to 20%.

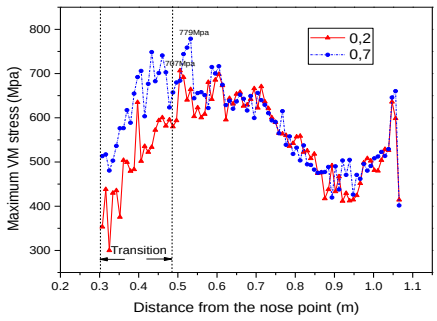

a

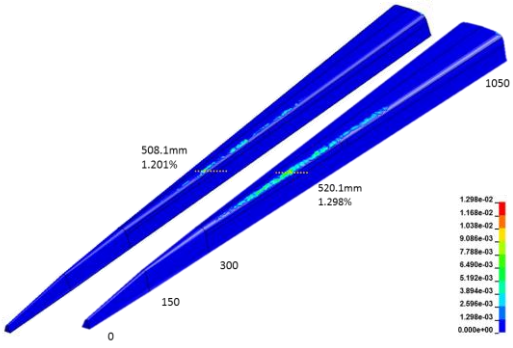

b

Figure 6. Results of friction coefficients variation: (a) maximum Von Mises stress, (b) effective plastic strain after one wheel passage

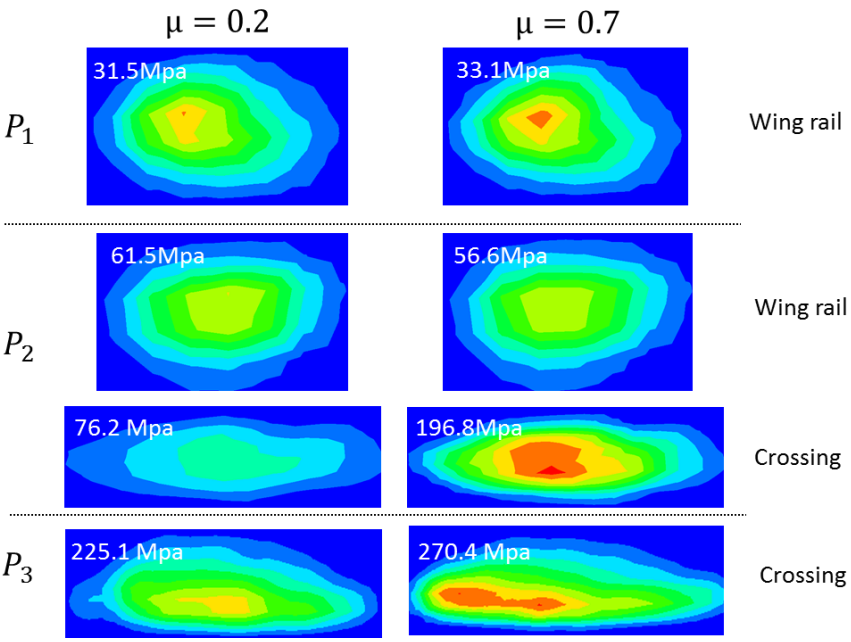

Figure 7. Results of friction coefficients variation: Surface shear stress at three position: P_1 = 72.2mm, before transition; P_2 = 325.0mm, in transition; P_3 = 577.7mm, after transition

Figure 8 presents the longitudinal contact force and friction energy dissipated at the wheel and rail interface, which are associated with wear and surface damage of the crossing. Figure 8a indicates that with μ = 0.7 the maximum longitudinal force significantly increases (41.2%) due to the high friction. In Figure 8b the frictional energy dissipation from both wheel-wing rail and wheel-crossing interface is plotted. It shows that with μ = 0.7 the maximum friction energy increases by 21.8%. The average of friction energy dissipation in the wing rail is approximately 0.02J, while it increases to 2.5J in the crossing due to the impact. It can be concluded that the high impact on the crossing may not only lead to the rolling contact fatigue problem, but also result in the increasing amount of wear.

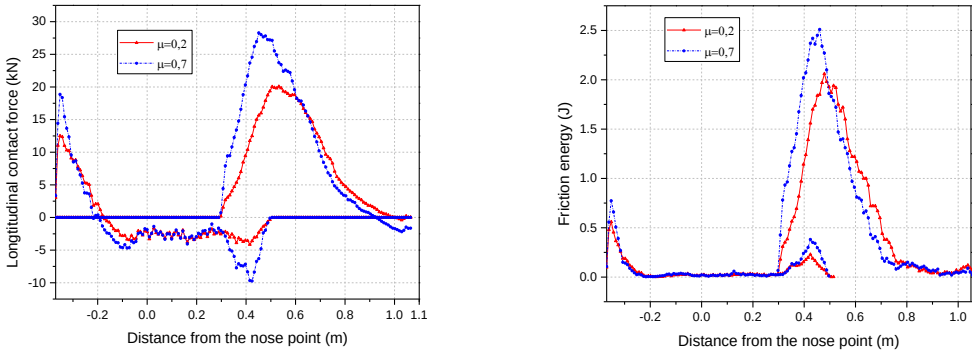

a b

Figure 8. Results of friction coefficients variation: (a) longitudinal forces, (b) friction energy dissipation

Since different friction conditions have great effect on surface stress state, the surface shear stress and surface pressure along the longitudinal axis at the critical positions ($\mu = 0.2$: P=507mm, $\mu = 0.7$: P=533mm) are of interest (Figure 9). It can be seen that the surface shear stress greatly increases (36.9%) by the high friction. Furthermore, comparing the contact patch in both cases where the maximum stress occurs, in the case of $\mu = 0.7$ it initiates more at the rear in the contact patch. The interface pressure in the case of $\mu = 0.7$ is slightly lower than $\mu = 0.2$, which can be explained by the larger plastic deformation caused by the high friction. Therefore, it can be concluded that the surface shear stresses are significantly affected by friction coefficient; however, it is not prominent in normal direction such as pressure distribution.

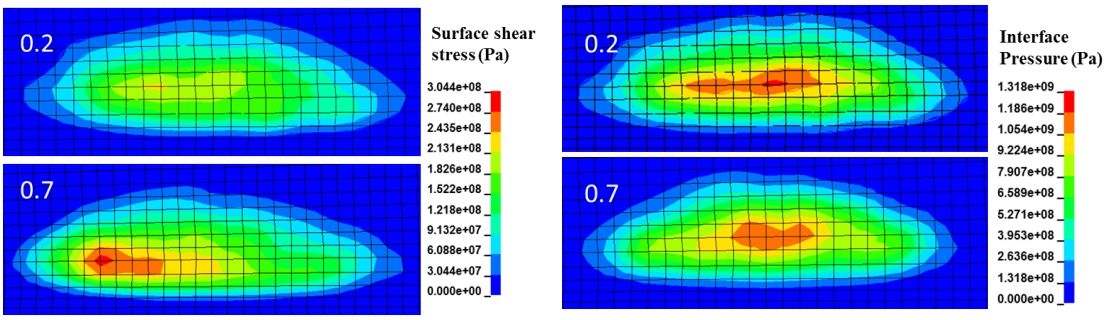

a b

Figure 9. Results of friction coefficients variation at critical positions: (a) surface shear stress, (b) interface pressure

4.3. Traveling directions

The contact forces in three directions and maximum VM stress in the crossing of both facing and trailing moves are presented in Figure 10. In the case of different traveling directions, the transition behaviour of the wheel and rail interaction is of

great importance. It can be seen from Figure 10a that the transition area is shifted backward in the case of trailing move (0.4m to 0.6m). After the transition at P=400mm the wheel generates a large impact on the wing rail (206kN), which is even greater than the impact on the crossing (176kN) in facing move. The increment of the impact forces reaches 17.0%. Figure 10b and 10c show that compared with the facing move, the wheel generates less lateral impact on the wing rail in the trailing move, while the longitudinal forces on the wing rail increase that result in larger surface shear stresses. The maximum VM stress shows the similar results that high VM stress is generated in the wing rail. It can be concluded that in the trailing move, high impact is generated on the wing rail and can be even larger than the one on the crossing in the facing move. The critical position (P_{cr}) in the trailing move is located on the wing rail at $P_{cr} = 400$mm from the nose point.

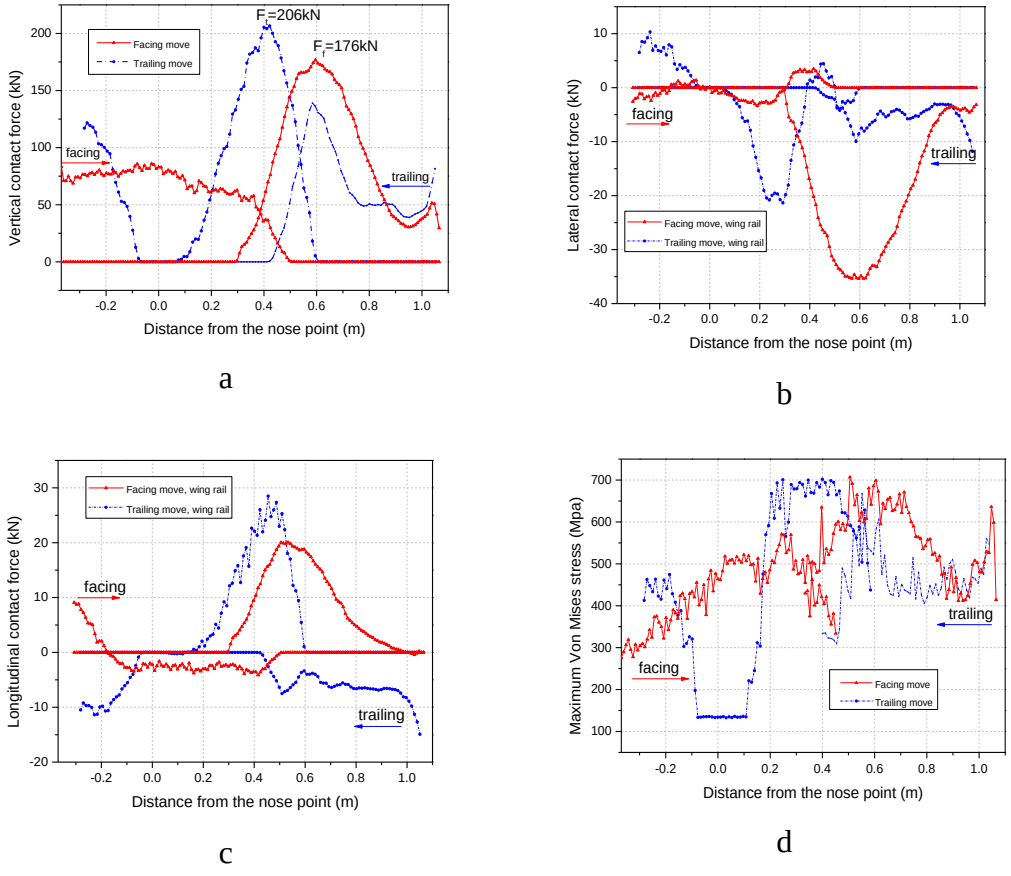

Figure 10. Results of traveling directions variation: facing move and trailing move: (a) vertical contact forces, (b) lateral contact force, (c) longitudinal contact force. (d) maximum VM stress

The transitions including the start (P_s) and end position (P_e) of the transition as well as the critical position (P_{cr}) on crossing or wing rail are selected as they are necessary to describe the wheel and crossing interaction during the wheel passage

(Figure 11). It can be seen that as discussed above, the transition (P_s to P_e) in the trailing move is shifted backward on the crossing, with similar transition length compared with the one in the facing move. However, the distance between P_e to P_{cr} is longer in the trailing move, which can be explained by the movement of the wheelset. In the trailing move, the wheel is climbing up from the crossing to the wing rail, because at those positions the wing rail is higher than the crossing. In contrast, in the facing move the wheel falls onto the crossing nose after the transition, which leads to the fast occurrence of the impact.

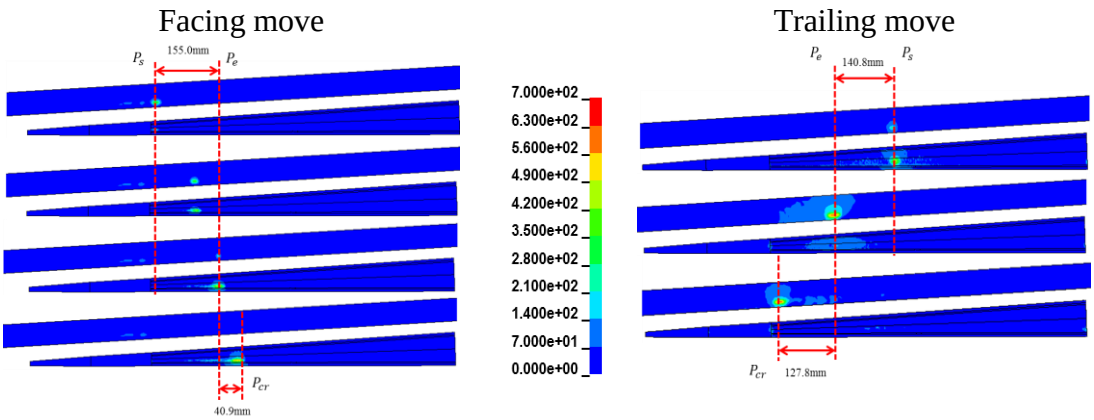

Figure 11. Transition behaviour under different traveling directions: (a) facing move, (b) trailing move

As for the wheel movement, the vertical and lateral displacements of the inner wheel (crossing side) are shown in Figure 12. It can be seen from Figure 12a that in both cases, the wheel has a vertical displacement of approximately 1.5mm after stabilization due to gravity and the applied axle load. In the facing move, due to the geometrical irregularities of the wing rail and the crossing, the wheel generates an impact on the crossing which results in the increment of the vertical displacement at around P=450mm. After the impact the wheel centre moves up again. While at the end of the simulation the wheel returns to the position that is higher than the original position, which can be explained by the fact that the wheel bounces on the rail due to the large impact. In the trailing move, the wheel continues lower its position since the height of the crossing decreases. After the transition (0.45m-0.6m) the wheel moves up and rolls on the wing rail. Similar as in the facing direction, the large impact on the wing rail results in the wheel bouncing, thus the wheel position goes down again. The lateral displacement of the wheel in trailing move shows that, different from the facing move that the wheel generates a large lateral movement and being pushed back, the wheel tends to follow the edge of the crossing nose until fully transferred to the wing rail. It also explains the smaller lateral contact forces in Figure 10b.

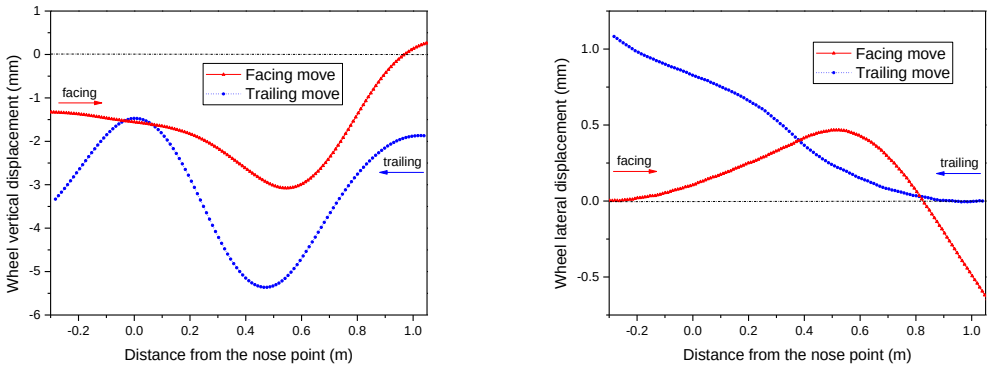

a b

Figure 12. Inner wheel transition behaviour under different traveling directions: (a) vertical wheel centre displacement, (b) lateral wheel centre displacement

5. Fatigue life analysis

Using the critical plane and energy density based fatigue model (Eq.1 and Eq.2), the fatigue life analyses of these three parameters are performed. Several locations on the crossing and wing rail are selected, including the critical position (with maximum VM stress) and four other equally spaced positions ($P_1, P_{cr}, P_2, P_3, P_4$), as shown in Figure 13a. P_1 locates before P_{cr}, while P_2 to P_4 locate after P_{cr}. It should be noted that according to the above results, the critical positions using soft pads (P_{cr-p}) and high friction (P_{cr-f}) are close to the one of the reference case (P_{cr}), as shown in Figure 13a. At each position, the element with the maximum VM stress is selected for the fatigue analysis ($E_1, E_{cr}, E_2, E_3, E_4$), that is to say, the fatigue analysis is performed at five elements at five different longitudinal positions. However, in the case of trailing move, the selected positions are different. The first three positions are on the wing rail, while the other two are on the crossing nose, which are shown in red in Figure 13a.

By the tensor rotation transformation of the stress and strain components, the FP value (Eq.1) for any plane of the selected element can be calculated. The plane with the maximum FP value is treated as the critical plane (crack initiation plane). At this plane two angles φ and θ are obtained (Figure 13b), which represent the spherical angles of the normal vector $\vec{n}$ of the critical plane to the coordinates system attached to the railhead surface. The angle φ represents the angle between the normal vector of the plane and the vertical direction of the rail, while the angle θ represents the angle between the normal vector and the lateral direction. To calculate the angles of the critical plane, the stress and strain values are used as input into the fatigue model, then the angle and the fatigue life to crack initiation are obtained for the three parameters.

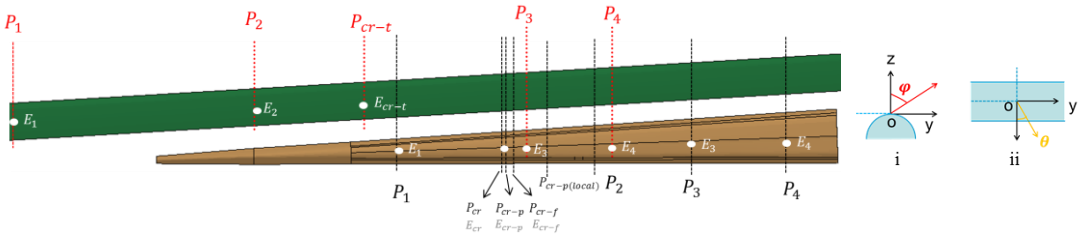

a b

Figure 13. Illustration of: (a) five selected positions on the crossing nose for fatigue analysis. (b) angles of the critical plane (crack initiation plane): (i) rail vertical cross section, (ii) rail longitudinal cross section

5.1.Elasticity of railpad

Figure 14a shows the six stress and strain components of $E_1, E_{cr}, E_2, E_3, E_4$ in cases v01 and v02. It can be seen that in both cases at different longitudinal positions (P_1 to P_4) the stress and strain states vary a lot, in which the components of E_{cr} reaches the highest value due to the impact. Among the six stress components, the variation of the vertical stress (σ_z) is the most significant, showing that by changing the railpad stiffness the vertical impact of the wheel is greatly varied, and is ultimately reflected in the variation of the stresses. It can be seen that in cases v01 and v02, the stress and strain components at P_1 and P_2 are comparable, while in V02 the components decrease at P_{cr} and increase at P_3 and P_4. These stress and strain components are used in the fatigue model to calculate the *FP* value and the number of cycles to fatigue crack initiation.

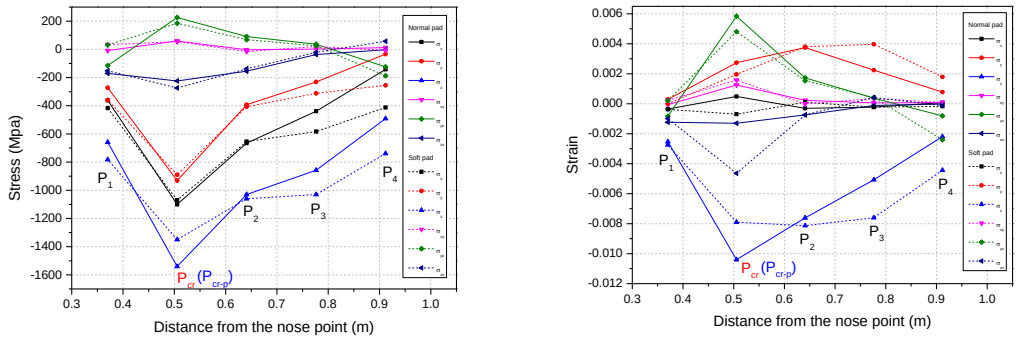

a b

Figure 14. Results of railpads stiffness variation (v01 and v02): stress and strain components at five selected elements: (a) stress components, (b) strain components

Figure 15a shows the angles of the critical planes of both cases. It can be seen that with different railpads stiffness, angles θ in both cases correlate well and lie in the range of [65°, 110°]. However, the pads stiffness greatly varies the angle φ at the positions in the middle part of the crossing (0.5m to 0.8m). Regarding to the fatigue

life prediction in Figure 15b, at P_1 and P_2 the fatigue lives slightly increase when using soft pads, especially at P_{cr}, the fatigue life increases from $N_r = 18{,}854$ cycles to $N_r = 33{,}542$ cycles. However, since the impact location is shifted further along the crossing using soft pads, the fatigue life of the crossing rear (P_3 and P_4) decreases, but it is not decisive for the service life of the crossing. Therefore, it can be concluded that when using soft pads the fatigue life of the crossing at the critical (impact) position can be increased.

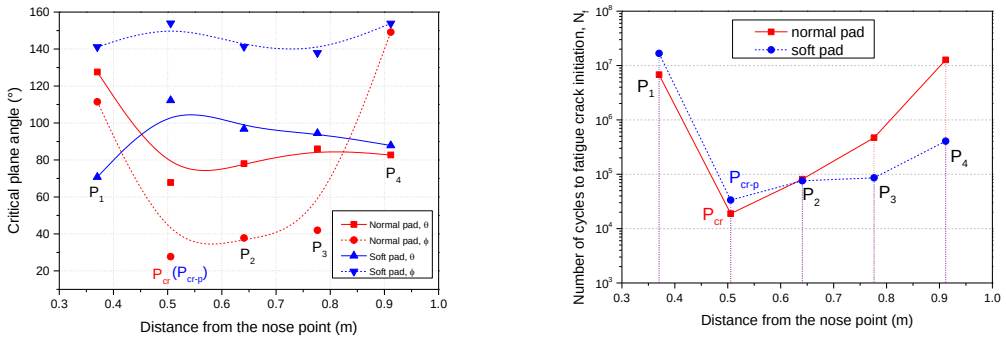

a b

Figure 15. Results of railpads stiffness variation (v01 and v02): fatigue life prediction of: (a) angles of the critical planes, (b) number of cycles to fatigue crack initiation

The crack planes angles and the fatigue life in case v03 that using the soft pads locally are shown in Figure 16. Regarding to the crack planes, angle θ in two cases that represents the angle between the normal vector and the lateral direction correlates well with each other, in which at P_1 is around 130° and at P_{cr} to P_4 lies in [60°, 95°]. However, similar to case v02, the angle φ that represents the angle between the normal vector and the vertical direction, differs a lot. The results of fatigue life prediction (Figure 16b) show that when using soft pads locally, the fatigue life at P_1 increases by more than five times. At P_{cr} the fatigue life increases slightly from $N_r = 18{,}854$ cycles to $N_r = 21766$ cycles. From P_{cr} to P_4 the fatigue life grows rapidly that at the crossing rear the fatigue life turns to be ten times larger than the one in case v01. Therefore, it can be concluded that although not all the selected positions have an increment in the predicted fatigue life, using soft pads only under the crossing nose has a benefit in increasing the fatigue life of crossing at the impact location as well as the crossing front and rear.

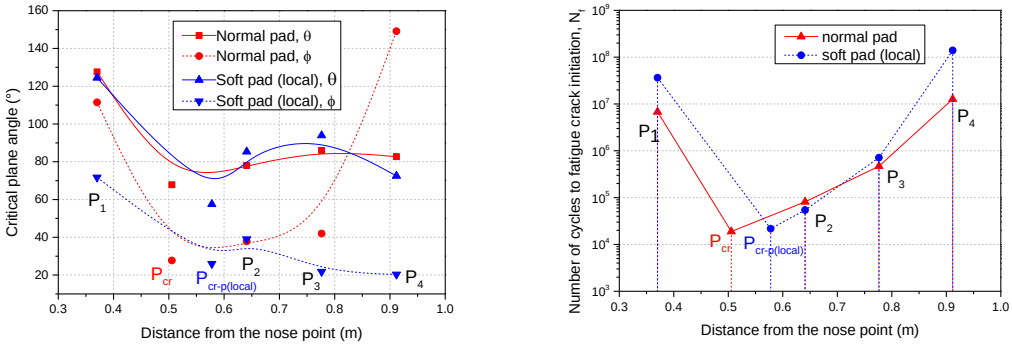

a b

Figure 16. Results of railpads stiffness variation (v01 and v03): fatigue life prediction of: (a) angles of the critical planes, (b) number of cycles to fatigue crack initiation

5.2.Friction coefficient

The stress and strain components with different friction coefficients are shown in Figure 17. It can be seen that different from the case with railpads stiffness variation, the vertical stress and strain (σ_z, ε_z) in both cases change little. However, the stress and strain in lateral (σ_y, ε_y) and longitudinal (σ_x, ε_x) direction have greater variation, which is corresponding to the results in Figure 9 and prove that the effect of the friction coefficient on the stress and strain state in tangent direction is much larger than the one in facing direction.

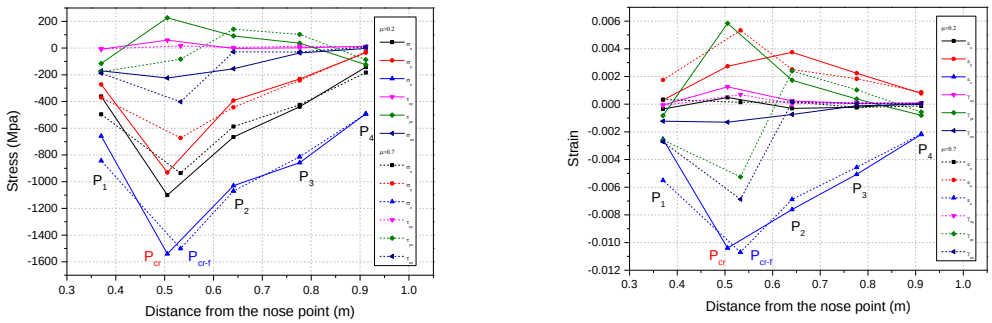

a b

Figure 17. Results of friction coefficients variation: stress and strain components at five selected elements: (a) stress components, (b) strain components

Figure 18a shows that the similar to the case of railpads stiffness variation, angles θ in both cases correlate well and mostly lie in [60°, 100°], while angle φ still has significant variation. The fatigue life prediction in Figure 18b presents that with $\mu = 0.7$, before the P_1 the fatigue life is shorter than the value with $\mu = 0.2$. Also at

P_{cr}, it can be seen that high friction leads to shorter fatigue life. After the impact, the fatigue lives in both cases are comparable, with slightly higher value with $\mu = 0.7$.

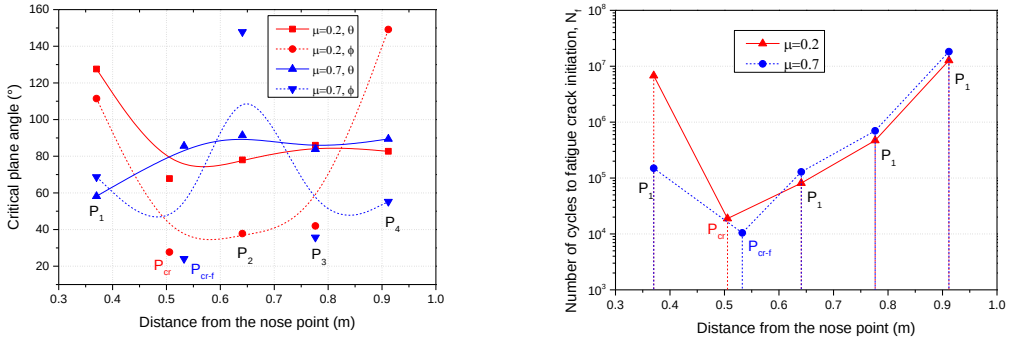

a b

Figure 18. Results of friction coefficients variation: fatigue life prediction of: (a) angles of the critical planes, (b) number of cycles to fatigue crack initiation

5.3. Traveling direction

As discussed above, since the transition and the impact position are different in trailing move, the selected positions are correspondingly changed and shown in Figure 13a by the red lines. In the case of trailing move, five positions $(P_1, P_2, P_{cr-t}, P_3, P_4)$ are selected, in which two positions (P_1, P_2) are before the critical position (P_{cr-t}), the other two (P_3, P_4) are after P_{cr-t}.

The stress and strain components are plotted in Figure 19. It can be seen that compared with the large stress and strain increment at P_{cr} in the facing move, in trailing move at P_{cr-t}, the increment is relatively small. However, the fatigue analysis in Figure 20b shows that at P_{cr} and P_{cr-t}, the fatigue lives of the crossing are comparable, which means that similar to the impact on the crossing in facing move, the wing rail is also subjected to high impact that leads to the short service life in the trailing move. However, the predicted angles of the critical plane in Figure 20a show that the angles of the critical plane in the wing rail differ greatly from the ones on the wing rail. Therefore, the RCF crack initiation in the wing rail should be considered separately from the crossing, especially in the track that exists most of the traffic in trailing direction.

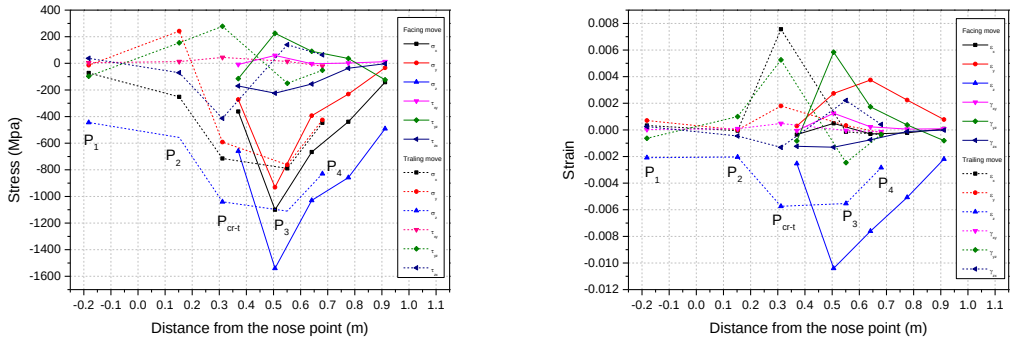

a b

Figure 19. Results of traveling direction variation: stress and strain components at five selected elements: (a) stress components, (b) strain component

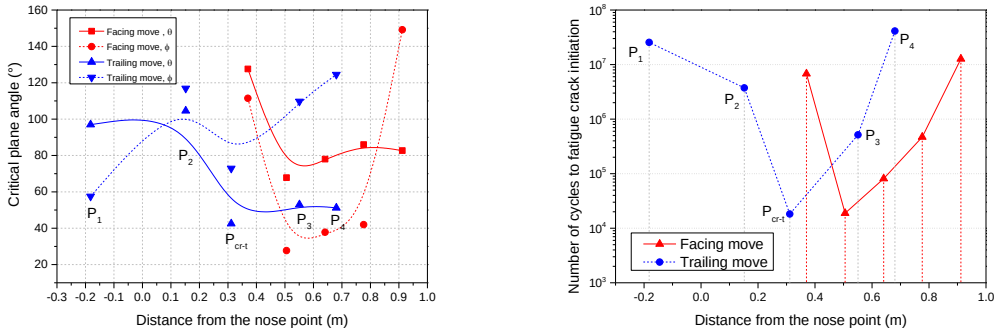

a b

Figure 20. Results of traveling direction variation: fatigue life prediction of: (a) angles of the critical planes, (b) number of cycles to fatigue crack initiation

6. Conclusion

In this paper, the parametric study on the wheel-crossing performance based on the dynamic analysis and fatigue life prediction of the crossing is performed. The effect of railpad stiffness, friction coefficients and traveling directions are investigated by the 3D explicit dynamic FE model of the wheelset moving over the crossing. The dynamic responses such as the contact forces in three directions, stress and strain in the rails and sleepers, friction energy dissipation as well as the transition behaviour are used to describe the crossing performance. Jiang and Sehitoglu fatigue model and the stress/strain life model are then employed for predicting the crack initiation planes and the number of cycles to fatigue crack initiation. The fatigue life of the crossing is used to assess the crossing performance of the three parameters.

The effect of railpads stiffness: at wheel-rail interface the impact forces and VM stress are reduced at the crossing front using soft pads. More importantly, the railpad stiffness has significant effect on the substructure, so that the stresses in the sleepers and ballast, especially the stress in the most critical sleeper, are greatly reduced by

the soft pad. However, at the crossing rear the value increases, since the impact location is shifted further along the crossing using soft pads. According to the fatigue analysis, using soft pads can slightly increase the fatigue life of the crossing. Furthermore, if varying the railpads stiffness only under the crossing nose, the initiation of the wheel-crossing contact is delayed so that the crossing front is subjected to less impact. The results of fatigue analysis also reveals that using soft pads locally has a benefit in increasing the fatigue life of crossing at the impact location as well as the crossing front and rear. Therefore, soft railpads should be applied under the crossing nose to reduce the impact on the crossing.

The effect of friction coefficients: high friction leads to larger VM stresses and shorter fatigue life in the transition area as well as the impact position. The surface shear stresses at these positions are significantly increased by the high friction, however, the contact pressure is not much affected. Moreover, regarding to the crack planes, the angles to the lateral direction in both cases correlate well, while the angles to the vertical direction have significant variation. After the impact position the fatigue lives in both cases are comparable, with slightly higher value with high friction.

The traveling directions: in the trailing move the transition area is shifted further on the crossing. After the transition, the wheel generates a large impact on the wing rail, which is even greater than the impact on the crossing in facing move. The transitions in both directions are investigated showing that in the trailing move it is shifted backward on the crossing, with similar transition length compared with the one in facing move. The fatigue analysis shows that compared with the ones on the crossing nose in the facing move, the crack initiation planes vary greatly on the wing rail in the trailing move. Moreover, the impact position on the wing rail is subjected to comparable short life as on the crossing nose in the facing move.

This study provides the insights on the effect of the analysed factors on the crossing behaviour, based on a fatigue life analysis. In the future work, the combination of these factors might be considered for specific loading conditions to improve the crossing performance.

7. Acknowledgements

This work has been sponsored by the Open-end Funds from Key Laboratory of High-Speed Railway Engineering, Ministry of Education, China.

8. Reference

[1] C. Wan, V.L. Markine, I.Y. Shevtsov, “Improvement of vehicle-turnout interaction by optimising the shape of crossing nose”, Vehicle System Dynamics, 52, 1517-1540, 2014.

[2] B.A. Pålsson, “Optimisation of Railway Switches and Crossings”, Doctoral thesis, Chalmers University of Technology, ISBN 978-91-7385-978-3.

[3] M. Pletz, W. Daves, H. Ossberger, “A wheel set/crossing model regarding impact, sliding and deformation-Explicit finite element approach”, Wear, 294-295, 446-456, 2012.

[4] L. Norberg, “Fatigue properties of austenitic Mn-steel in explosion depth hardened condition”, Master Thesis, Chalmers University of Technology.
[5] L. Xin, V.L. Markine, I.Y. Shevtsov, “Simulation of Railway Crossing Damage Due to Welding Defect”, The Second International Conference on Railway Technology: Research, Development and Maintenance, (Civil-Comp Press, Ajaccio, France, 2014).
[6] V.L. Markine, M.J.M.M Steenbergen, I.Y. Shevtsov, “Combatting RCF on switch points by tuning elastic track properties”, Wear, 271, 158-167, 2011.
[7] C. Wan, V.L. Markine, I.Y. Shevtsov, “Optimization of the elastic properties of turnout crossings”, Proc IMechE, Part F: J. Rail and Rapid Transit, doi:10.1177/0954409714542478, 2014.
[8] Y. Zhu, “Adhesion in the wheel-rail contact, Doctoral thesis”, KTH Royal Institute of Technology, 2013.
[9] J. Suzumura, Y. Sone, A. Ishizaki, D. Yamashita, Y. Nakajima, M. Ishida, “In situ X-ray analytical study on the alteration process of iron oxide layers at the railhead surface while under railway traffic”, Wear. 271, 47–53, 2011.
[10] B.A. Pålsson, J.C.O. Nielsen, “Wheel–rail interaction and damage in switches and crossings, Vehicle System Dynamics”, 50, 43–58, 2012
[11] X. Liu, V.L. Markine, I.Y. Shevtsov, “Performance study of a double crossover for facing and trailing directions”, Proceedings of the 24th International Symposium on Dynamics of Vehicles on Roads and Tracks (IAVSD 2015) in Graz, Austria.
[12] M. Pletz, W. Daves, H. Ossberger, “A wheel set/crossing model regarding impact, sliding and deformation-Explicit finite element approach”, Wear, 294-295, 446-456, 2012.
[13] L.Xin, V.L. Markine, I.Y. Shevtsov, Numerical analysis of rolling contact fatigue crack initiation and fatigue life prediction of the railway crossing, Published online before printed, Wear, DOI:10.1016/j.wear.2016.04.016.
[14] L. Xin, V.L.Markine, I.Y. Shevtsov, Numerical analysis of the dynamic interaction between wheelset and turnout crossing using explicit finite element method, Vehicle System Dynamics, 54, 301-327, 2016.
[15] Y. Jiang, H. Sehitoglu, A model for rolling contact failure, Wear, 224, 38-49, 1999.
[16] M. Fermer, J.C.O. Nielsen, “Vertical interaction between train and track with soft and stiff railpads-full-scale experiments and theory”, Proc IMechE, Part F: J. Rail and Rapid Transit , 209 (1), 39-47, 1999.
[17] R. Lewis, U. Olofsson, “Wheel-rail interface handbook”, Woodhead publishing limited, 2009.